Sensors and Materials, Vol. 36, No. 8 (2024) 3419–3431
MYU Tokyo

S & M 3741

Fracture Mechanisms of Lead Zirconate Titanate Piezoelectric Thin Films Determined by Mechanical and Electrical Cyclic Loading Tests

Yuga Kumakiri,[1] Tomohiro Date,[2] Noriyuki Shimoji,[2]
Koji Terumoto,[2] and Takahiro Namazu[1,*]

[1]Kyoto University of Advanced Science, 18 Yamanouchigotanda-cho, Ukyo-ku, Kyoto 615-8577, Japan
[2]Rohm Co., Ltd., 21 Saiinmizosaki-cho, Ukyo-ku, Kyoto 615-8585, Japan

(Received May 23, 2024; accepted July 2, 2024)

Keywords: PZT film, dielectric withstand voltage, cyclic loading test, cracking, short circuit, fracture mechanism

In this paper, we describe the fracture mechanisms of lead zirconate titanate (PZT) piezoelectric thin films synthesized by sol-gel processing. One of the technical concerns in piezoelectric thin films is how their surface fractures because, in most cases, the films fail electrically, and the fracture surface is remade after its first fracture. To estimate the failure mechanisms, cantilever-type and clamped capacitor-type actuators made of PZT piezoelectric thin films deposited on a Si wafer were prepared and subjected to electrical and mechanical stresses. The cantilever-type actuators showed a decreasing trend in dielectric withstand voltage with increasing number of mechanical loading cycles. The clamped capacitor-type actuators showed a decreasing trend in withstand voltage with increasing cyclic voltage amplitude. Through mechanical and electrical experiments, we found that the origin of cracking differed from that of short circuit. This finding indicates that the PZT films fractured mechanically, then fractured electrically. The focused ion beam fabrication of a surface defect and scanning electron microscopy observation around the defect suggest a reasonable fracture mechanism.

1. Introduction

A lead zirconate titanate (PZT) film is well known as a representative piezoelectric film, which is utilized as an actuator in MEMS. The applications of the PZT MEMS include microactuators,[1–4] mechanical sensors,[5,6] energy harvesters,[7–11] ultrasound transducers,[12,13] and others.[14–17] The PZT's piezoelectric effect is used for passive applications, such as mechanical sensors and energy harvesters, whereas its inverse piezoelectric effect is used for active applications, such as microactuators and ultrasound transducers. One of the advantages of the use of PZT in MEMS is that it enables us to move micromechanical elements rapidly at more than several tens of kHz in the case of using thin PZT films. Another advantage is that thick PZT films can provide high power density, which can be utilized for energy-harvesting devices and

*Corresponding author: e-mail: namazu.takahiro@kuas.ac.jp
https://doi.org/10.18494/SAM5153

ISSN 0914-4935 © MYU K.K.
https://myukk.org/

high-power actuators, owing to an increase in the active volume of the films. In addition, thicker films tend to be less clamped to the substrate, which allows for higher domain wall mobility and may enhance their piezoelectric response. Considering the practical use of PZT films as functional materials, such rapid response and high-power output are really attractive, which is considered to be the main reason why the PZT films are being widely used as actuators in MEMS. Moreover, the PZT films can be produced relatively easier than other functional materials, such as shape memory alloys[18,19] and ferromagnetic and exothermic reactive films,[20,21] by the sol-gel method and sputtering.

In considering the mechanical reliability of PZT MEMS devices, one of the significant concerns in the PZT MEMS is that it is very difficult to understand how it fractures during operation.[22–33] If the PZT film is used as an actuator, a voltage is applied to the film for actuation. During the operation at a high voltage, the PZT MEMS suddenly collapses. After the rupture, the PZT MEMS changes shape within a very short period of time, and an irregular pattern can be observed as if the PZT film is partially melted. This means that the PZT MEMS fractured owing to both electrical and mechanical issues. Commonly, the fracture mechanism of hard materials such as metals and ceramics is discussed through the observation of the fracture surface where significant information, such as crack initiation, crack propagation, and fatigue striation, is included. In the case of MEMS devices with a PZT actuation mechanism, however, no marks remain on the fracture surface because second-order fracture occurs, which means that the evidence explaining the fracture disappeared completely. Therefore, it is challenging to correctly understand how the PZT MEMS failed in experiments. At the same time, revealing the fracture mechanism is of considerable interest to material researchers investigating the mechanical reliability of PZT MEMS devices.

The objective of this study is to clarify the fracture mechanism of PZT MEMS devices based on experimental findings. Two types of MEMS device with an actuation mechanism using the PZT film produced by the sol-gel method were prepared. A cantilever-type PZT MEMS device was subjected to cyclic mechanical loading, whereas a clamped capacitor-type PZT MEMS device was subjected to cyclic electrical loading. On the basis of experimental results derived from the two loading tests, a reasonable fracture mechanism is discussed from the viewpoint of the difference between the origins of electrical and mechanical fractures.

2. Specimen

Figures 1(a) and 1(b) show schematics of the cantilever-type and clamped capacitor-type PZT MEMS devices used for fracture mechanism investigation, respectively. The cantilever-type PZT MEMS device chip has multiple cantilever arrays with a width of 560 μm and lengths of 500–2000 μm, which consists of the PZT film actuator, upper and lower electrode layers, and Si substrate covered with SiO_2 film. The clamped capacitor-type PZT MEMS device has almost the same configuration other than its in-plane shape and non-self-standing property. The clamped capacitor of the PZT film has a circular shape with a diameter of 2800 μm. The two devices are produced through almost the same fabrication process flow, which is explained as follows: An n-type silicon-on-insulator (SOI) wafer with a 20 μm active layer, a 1.5 μm buried oxide (BOX)

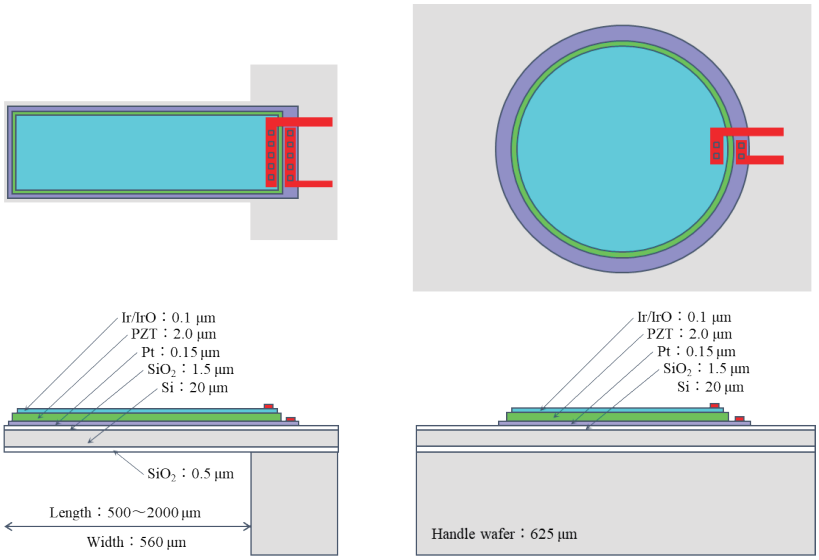

(a) Cantilever-type PZT MEMS (b) Clamped capacitor-type PZT MEMS

Fig. 1. (Color online) Schematics of the cross sections of PZT MEMS devices: (a) cantilever type and (b) clamped capacitor type.

layer, and a 200 μm handle layer is employed as a starting material. As the first step, wet oxidation is carried out to grow a SiO_2 layer of 1.5 μm thickness on the entire surface of the wafer. After that, a 0.15-μm-thick Pt film used as the lower electrode is deposited on the top surface of the wafer by sputtering. On the Pt film layer, a 2.0-μm-thick PZT film is deposited by the sol-gel method, followed by sputtering a 0.1-μm-thick Ir/IrO film onto the PZT film layer. The Ir/IrO film is utilized as the upper electrode. After these deposition processes, a device pattern for each layer from the upper electrode to the lower electrode is formed. The three layers are patterned one by one by photolithography using a positive photoresist and then etched by plasma etching using a photoresist mask. Then, an Al film is deposited on the top surface and patterned for making a wiring to apply an electrical voltage to the two electrode layers. In the case of the clamped capacitor-type PZT MEMS device, the fabrication is complete because no self-standing processes are necessary. In the case of the cantilever-type PZT MEMS device, the cantilever shape is processed from the top surface using photolithography and Si dry etching techniques. After the surface micromachining processes, Si dry etching from the back side of the wafer is carried out to produce a through hole to make the cantilever actuator structure self-standing. Finally, by dry etching the BOX layer to be removed, the self-standing cantilever-type PZT MEMS device is complete and ready for the fracture test.

3. Cantilever Fracture Testing

To experimentally investigate how mechanical loading affects the withstand voltage of the PZT film layer, the cantilever-type PZT MEMS devices were subjected to mechanical and

electrical loading cycles. First, quasistatic cantilever bending tests were performed to measure the force value where the PZT MEMS device fractures mechanically. Cantilevers with lengths longer than 1200 μm were chosen, and a normal force was applied at the point where the distance from the fixed end was only 1000 μm in all the samples using a tungsten probe from the overhead on the PZT film side until fracture, which indicates that tensile stress was generated in the film during the bending test.[34–36] A load cell with a capacity of 2 N was placed beneath the device chip to measure the applied force. Figure 2(a) shows a representative bending force–time relationship obtained in the cantilever bending test. The bending force was applied manually under the conditions of 2.5 mN loading step and 5 s holding time. It was found that the bending force–time relationship is almost linear at an almost constant loading speed, although it was applied by hand. At 63.8 mN, the applied force dropped considerably, which indicates that the device fractured mechanically in a brittle manner. In this study, five samples in total were subjected to the quasistatic bending test, and they fractured at the bending force ranging from 60.1 to 64.0 mN (mean: 63.7 mN), although those data are omitted here.

As a second step, cyclic mechanical loading was applied to the PZT MEMS devices. The cyclic mechanical load with a triangle waveform was applied manually using a tungsten probe. The maximum bending force was set to be 47.9 mN, which is 75% of the mean force where the PZT MEMS devices failed mechanically under quasistatic tension. As shown in Fig. 2(b), which is the partial data of the test, a triangle waveform of the applied bending force can be confirmed regardless of manual force application. We attempted to maintain the frequency and maximum force to be around 0.04 Hz and 47.9 mN, respectively, as much as possible. The cyclic bending loading was applied until 46 and 75 cycles. After 0, 46, and 75 loading cycles, three samples for each were subjected to the withstand voltage evaluation experiment. Figure 3 shows the relationship between the withstand voltage and the number of loading cycles. Before applying bending loading to the PZT MEMS device, the device failed when a voltage of 132 V on average was supplied between the upper and lower electrode layers. The voltage when the device failed electrically was judged as the withstand voltage of the device without any mechanical damage. With increasing number of loading cycles, the withstand voltage was found to decrease

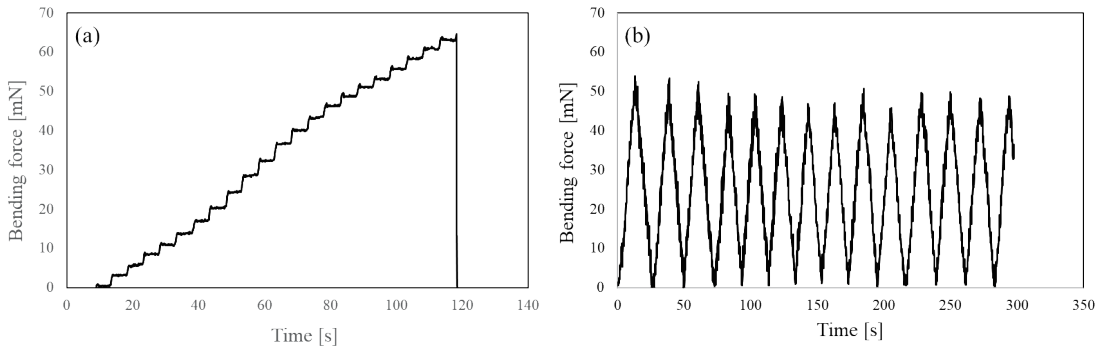

Fig. 2. Representative results of mechanical loading tests: (a) bending force–time relationship in quasistatic bending test and (b) bending force–time waveform in cyclic bending test.

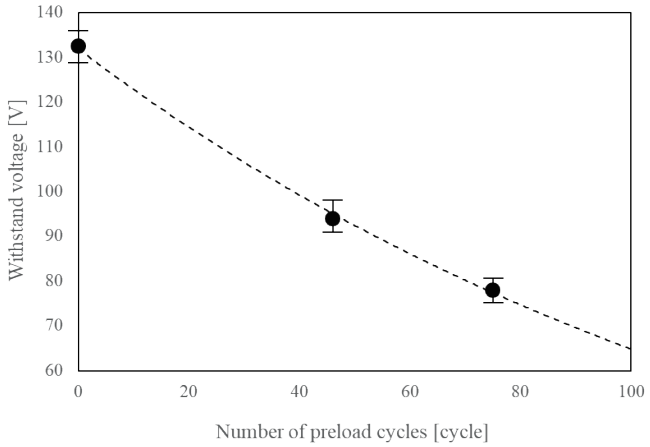

Fig. 3. Relationship between withstand voltage and number of mechanical preloading cycles.

monotonically. After 75 mechanical loading cycles, it was 80 V on average, which is around 60% of the initial value. In this case, the withstand voltage (V_w) decreased with increasing number of loading cycles (N) at $V_w = 132e^{-0.007N}$, which strongly indicates that cyclic mechanical loading affected the electrical reliability of the PZT film used in the MEMS device.

Figure 4 shows a magnified SEM image taken around the cracking part along with the energy dispersive X-ray (EDX) analysis results. In this experiment, the cantilever device was broken mechanically when the withstand voltage was applied. In the vicinity of the fractured part, a crack was observed as seen in the CCD image shown in the upper-right side of the figure. In the SEM image, the crack was found to be introduced in the PZT film layer. It propagated from the crack initiation part, which is probably the fractured portion of the cantilever device, to the cantilever's sidewall. Note that the portion around the crack only appears melted and the melted portion continues along the crack. That is, a crack that we observed in the CCD image was represented as the combination of the crack and melted materials along the crack. In the cross section of the cantilever device, both the columnar layer and the flat portion can be seen. The former is the non-melted PZT film layer and the latter is the melted portion. According to the EDX analysis results, if oxygen is excluded, the melted material, part B, contained large amounts of Pb, Zr, and Ti, which are the major components of the PZT film indicated as part A. Ir and Al, which are respectively used as the upper electrode and wiring materials in the device, were included in the melted region. Those EDX results imply that, by supplying a voltage around its withstand voltage, the PZT film layer was melted and the cantilever device was broken mechanically. However, the correlation between PZT melting and cracking is still unknown in this experiment.

4. Clamped Capacitor Fracture Testing

To understand the correlation between electrical degradation and mechanical cracking, the effect of cyclic electrical loading on the fracture of the PZT film layer was examined using the

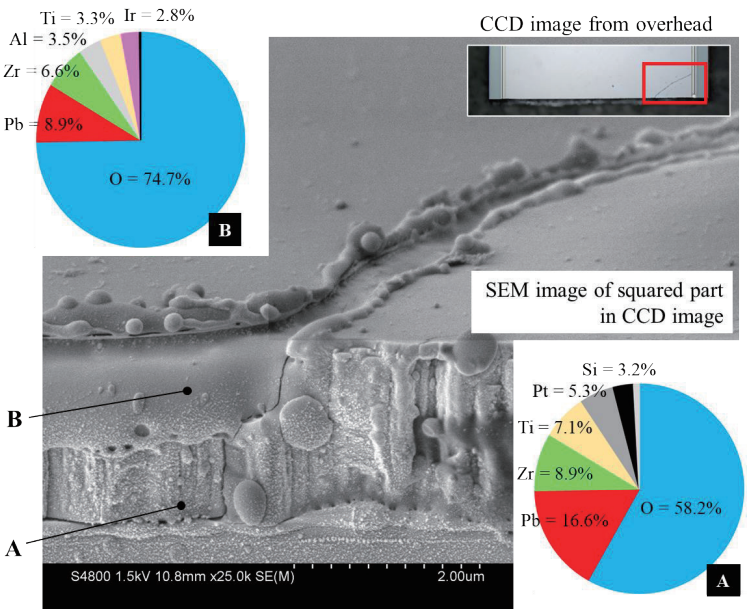

Fig. 4. (Color online) SEM image of failed PZT MEMS device along with ED-analyzed material element percentage at columnar PZT film and melted portion.

clamped capacitor-type PZT MEMS devices. The main reason why the clamped capacitor-type PZT MEMS devices were chosen is that, in the latter, the area of the PZT film was larger than that in the cantilever-type devices, which allows an easier observation of the degradation of the PZT layer. First, cyclic electrical loading was applied to the PZT MEMS devices to observe the surface degradation of the PZT film. The voltage amplitude was set to 0, 50, 75, and 100 V, and the loading frequency was maintained at 50 Hz. Each loading was applied until the number of loading cycles reached 1,000,000. After the cyclic loading tests, a quasistatic electrical loading test was carried out at a constant rate of 0.5 V/s to evaluate the withstand voltage of the PZT film. Figure 5 shows the relationship between the voltage amplitude in the cyclic loading test and the withstand voltage. Three samples were subjected to the experiment under each voltage amplitude condition. Before cyclic electrical loading, the PZT MEMS device failed electrically when 216.5 V was applied on average. This voltage is the withstand voltage of the PZT film. With the increase in amplitude to 50 V, the mean withstand voltage decreased to 149.5 V, which is roughly 70% of the initial value. The withstand voltage (V_w) was found to decrease monotonically with increasing voltage amplitude (V_A), which can be expressed as $V_w = 210e^{-0.005VA}$. This relationship implies that the PZT MEMS device's performance, showing the withstand voltage, is determined by cyclic electrical loading as well as cyclic mechanical loading because the PZT film was subjected to cyclic mechanical stress originating from cyclic electrical voltage application.

After the PZT MEMS failure during the quasistatic electric loading test, the PZT film surface was observed with a CCD camera as shown in Fig. 6 [voltage amplitudes of (a) 0, (b) 50, and (c) 75 V during cyclic electrical loading test]. With the voltage amplitude of 0 V indicating no cyclic

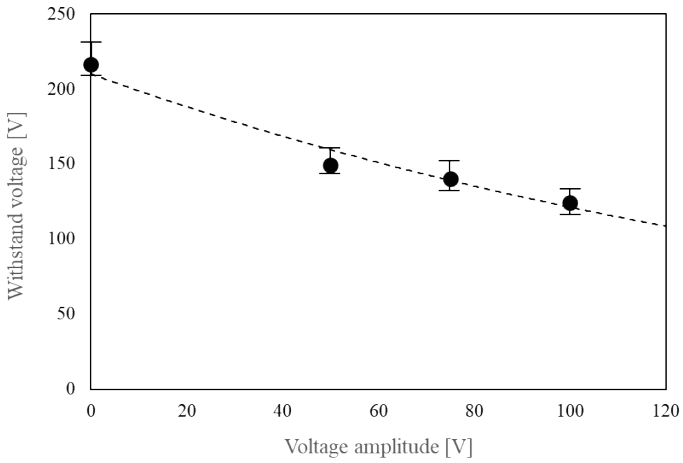

Fig. 5. Relationship between withstand voltage and voltage amplitude during cyclic electrical preloading test.

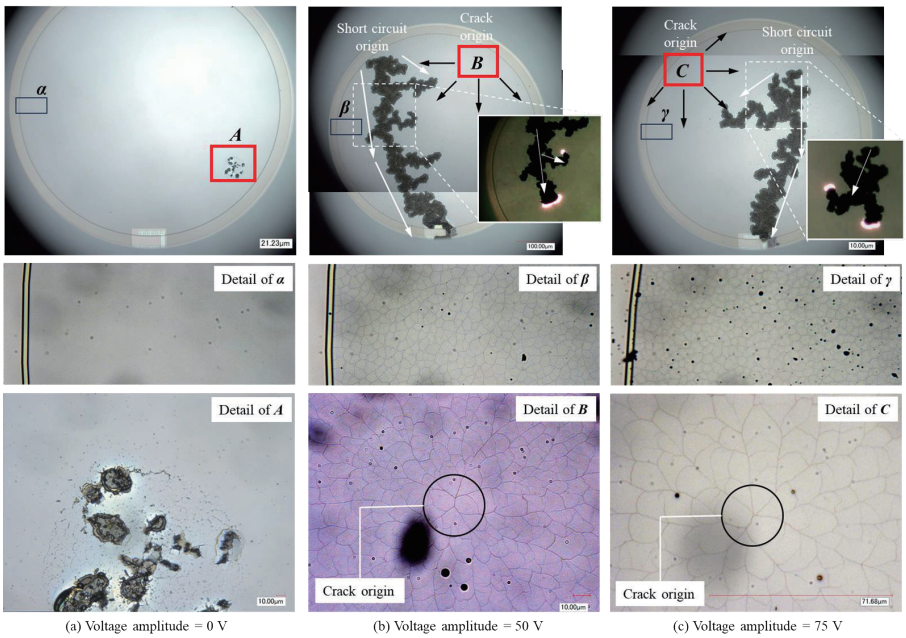

(a) Voltage amplitude = 0 V (b) Voltage amplitude = 50 V (c) Voltage amplitude = 75 V

Fig. 6. (Color online) Representative membrane surface observation results after withstand voltage evaluation tests. After a cyclic electrical preloading test at voltage amplitudes of (a) 0, (b) 50, and (c) 75 V, the dielectric withstand voltage was measured by quasistatic electrical loading.

electric loading, even though the device fractured, the PZT film showed almost a flat surface except for one portion indicated as A. In the magnified image (second row), some gray dots on the flat surface were found, which are dust on the lens of the CCD system. In the detailed image of A (third row), several dark color regions can be seen. It is considered that the PZT MEMS device failed at portion A where the PZT film was melted when 216.5 V was applied. Around those portions, it can be observed that very small cracks were introduced. On the other hand, the

PZT MEMS devices tested with the voltage amplitudes of 50 and 75 V showed similar trends. In the images of the entire surface (first row), a dark color fluctuating pattern like a snake can be clearly seen. According to the snapshot taken during the quasistatic electrical loading test, the pattern made was found to be due to the electric short circuit. Figure 4(b) shows that the short circuit started from the point in the upper left portion and then propagated to the bottom side where the electrode existed. As shown in Fig. 4(c), the same phenomenon started from the upper right point and then propagated to the electrode as well. The interesting thing about this is that the propagation direction was split into two in the middle and one of the two stopped. This implies that once one short circuit reached an electrode, the other one stopped immediately, and the short circuit phenomenon observed in this study finished in a very short time. From the experimental findings, it can be confirmed that those devices finally fractured electrically. The portion of the surface other than the trail of electrical short circuit apparently appears flat in the entire surface image. However, the magnified images (second row) depict that there are so many cracks introduced into the entire surface of the clamped capacitor actuator. One island made by cracking measures almost 10 μm in planar diameter, which seems to consist of multiple crystal grains. On the PZT capacitor surface, small black dots were detected. Those are considered as the particles of melted material flown in all directions when the electric short circuit occurred very rapidly. The number of particles appeared to increase when the voltage amplitude was increased to 75 V, indicating that the short circuit probably occurred with a large impact. In the detailed images of B and C (third row), note that multiple cracks on the two devices started from only one point, indicated as the center of the solid circle in each image. The multiple cracks would have started at the center of the circle, which was the origin of the cracks, and then would have propagated radially. Furthermore, one more important finding is that the origin of the cracks was definitely different from that of the electrical short circuit. That would be strong evidence that the PZT MEMS devices degraded both mechanically and electrically with the application of cyclic electrical loading to the PZT film. Also, it can be considered that the two experimental findings, namely, radial crack propagation and the difference between the origins of the mechanical and electrical degradations, suggest that mechanical cracking might have occurred first, followed by the electrical short circuit.

As shown in the cross-sectional image in Fig. 7(a), the crack is found to have penetrated the top Ir/IrO electrode and PZT actuation layers, and not to have penetrated the bottom Pt electrode layer and the SiO_2 layer beneath the bottom electrode. With careful observation, the width of the crack in the PZT layer was found to be larger than that in the top electrode layer. The PZT film and the two electrode metals are well known as brittle and ductile materials, respectively. Thus, the difference in crack width implies that the cracks observed on the PZT capacitor surface were introduced into the PZT layer first, then immediately propagated into the top electrode layer. Since the bottom Pt electrode layer was tightly restrained to the SiO_2 film, the cracks would not have propagated to the bottom electrode. According to Fig. 7(b) showing the cross-sectional image taken where the electric short circuit occurred, it was found that the PZT film was melted and the melted material was put on the PZT capacitor as with the cantilever-type PZT MEMS device already shown in Fig. 4. No visible cracks could be detected in the cross section where the short circuit occurred. Even from this experimental finding, it can also be considered that the

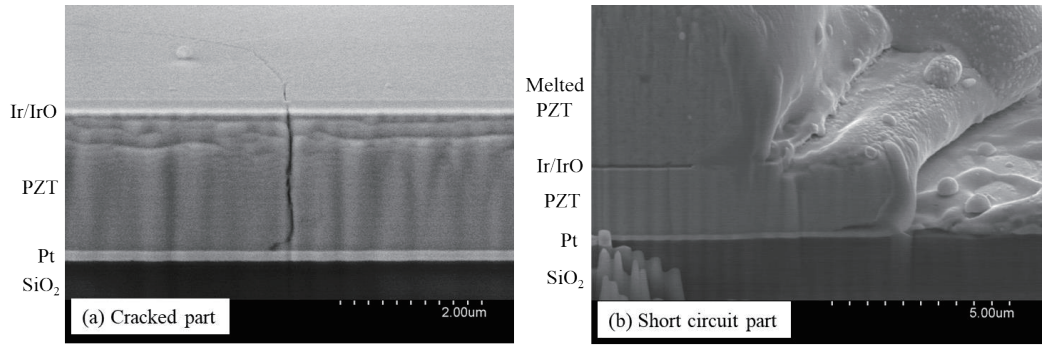

Fig. 7. SEM images of cross section of failed PZT MEMS device after quasistatic electrical loading test: (a) cracked and (b) short circuit portions.

electrical short circuit might have occurred after the mechanical cracking has been introduced into the PZT film, although no direct evidence to explain this could be obtained in the experiment. To experimentally explain which occurred first, an electrical short circuit or mechanical cracking, an artificial mechanical defect was processed by focused ion beam (FIB) fabrication on the PZT MEMS device. Figure 8 shows a schematic of the FIB-processed mechanical defect along with the photograph. A focused Ga ion beam at the acceleration voltage of 30 kV was irradiated from overhead of the PZT capacitor surface until the fabrication depth reached the Si handle wafer. By shifting the fabrication portion while gradually decreasing the acceleration voltage, a slope was produced to easily observe the cross section of the fabricated vertical wall. The artificial defect was 200 μm in width and 5 μm in depth at the deepest portion. On the FIB-processed surface, a river-like pattern can be observed as if water flows from the top surface to the inside. It might be cracks introduced into the PZT film layer owing to external energy application originating from FIB irradiation.

After fabricating the artificial mechanical defect, static electrical voltage was applied between the upper and lower electrodes until failure. The representative observation results obtained after the application of electrical voltages of 0, 15, and 20 V are shown in Figs. 9(a)–9(c), respectively. In Fig. 9(a), the PZT capacitor surface just after the defect fabrication appears flat without any other defects. In the magnified image of D, however, cracks were found to be introduced entirely onto the top surface of the capacitor. The crack density of the clamped capacitor after the FIB fabrication seems to be lower than that after the cyclic and quasistatic electrical loading tests shown in Figs. 6(b) and 6(c). After applying 15 V, as shown in the first-row image in Fig. 9(b), it appears like nothing occurred. However, as seen in the detailed image of D (second row), one portion of the sidewall deformed slightly as if it started to melt. The sidewall of the fabricated mechanical defect other than the melted portion had many particle-like convexes, indicating that the PZT film layer started degrading arising from the application of 15 V. In addition, new small debris were found to be attached to the PZT capacitor surface especially around the melted portion. After the voltage application of 20 V, in the entire surface image of the clamped capacitor shown in Fig. 9(c), it was clearly found that the electrical short circuit formed, which started from the edge of the artificial mechanical defect to the electrode.

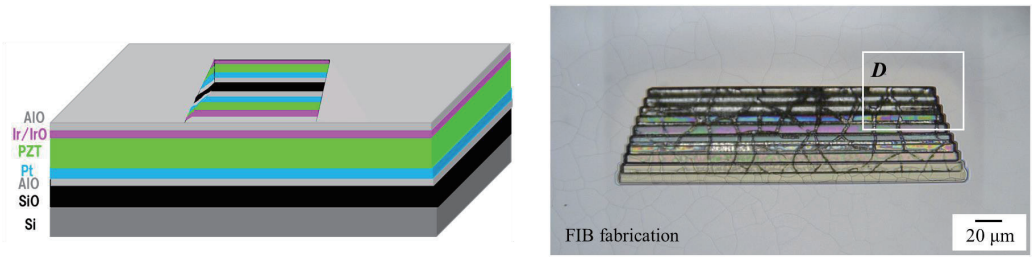

Fig. 8. (Color online) Schematic of artificial mechanical defect produced by FIB process along with the photograph of the produced defect on the membrane-type PZT MEMS device.

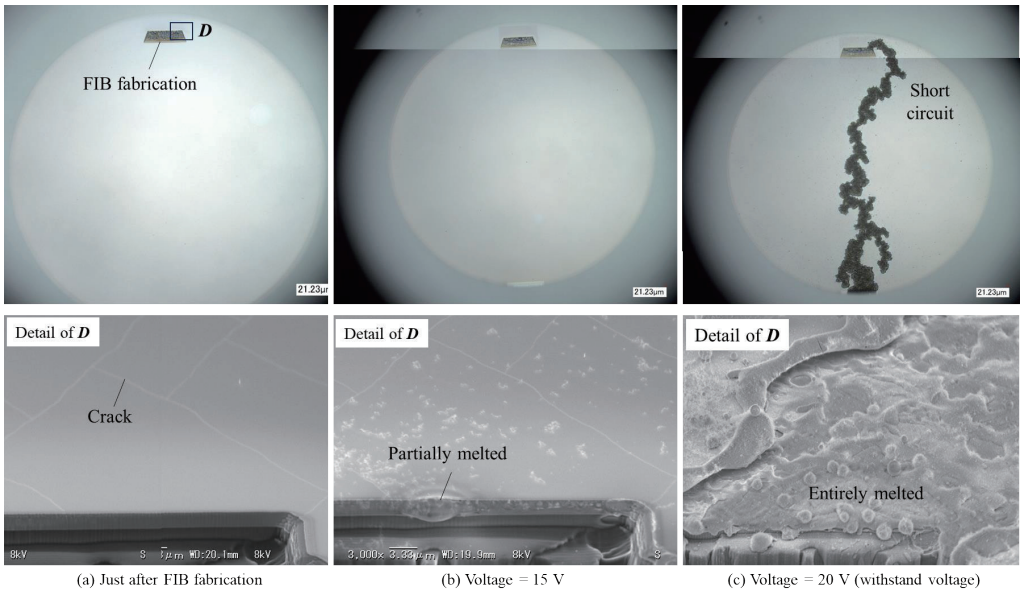

(a) Just after FIB fabrication (b) Voltage = 15 V (c) Voltage = 20 V (withstand voltage)

Fig. 9. (Color online) Representative membrane surface observation results: (a) just after FIB fabrication and quasistatic electrical voltage application at (b) 15 and (c) 20 V. At 20 V application, short circuit occurred in the PZT MEMS device, indicating that 20 V was the dielectric withstand voltage of the device.

In the detailed image of D (second row), the defect structure completely collapsed and the PZT film melted from the partially melted portion, as found from the magnified image in Fig. 9(b), to the outside radially. After the melting phenomenon was observed, it was confirmed that no new cracks were introduced into the clamped capacitor. The PZT MEMS device with the artificial mechanical defect collapsed at 20 V, which means that the device's withstand voltage was 20 V. Initially, the device exhibited the withstand voltage of 216.5 V, which gradually decreased to 124.5 V with increasing voltage amplitude to 100 V in the cyclic electrical loading test. The withstand voltage obtained in this experiment was 20 V, which is very low, roughly one-sixth to one-eleventh of the values obtained under cycling electrical loading conditions. The number and magnitude of mechanical damage before the short circuit occurs directly determine the durability of the PZT MEMS device to the applied voltage for actuating the device. That is,

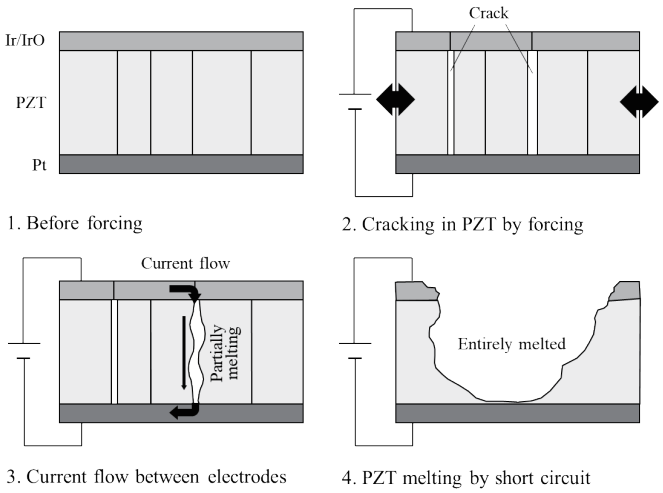

Fig. 10. Schematic of fracture mechanism of PZT MEMS device. By applying external force, the PZT film is subjected to stress, and then cracks are introduced into the film. Current flows on the crack surface; consequently, the PZT film melts, leading to short circuit in a very short period of time.

through the experiment with the introduction of an artificial mechanical defect using FIB, we confirmed that the electrical short circuit leading to catastrophic failure would have occurred after mechanical cracking had been introduced into the PZT film layer.

The fracture mechanism of the PZT MEMS device is summarized in Fig. 10 on the basis of the experimental findings obtained in this study. The PZT film has a columnar polycrystalline structure sandwiched by the upper and lower electrode layers made of Ir/IrO and Pt, respectively. Once stress is applied to the PZT film by cyclic volume shrinkage originating from cyclic electrical voltage applications or by direct cyclic mechanical forcing, cracks are introduced into the PZT film because of its brittleness. Then, the cracks easily propagate into the upper and lower electrode layers because these layers are directly attached to the PZT film. At the high electrical voltage applied between the two electrode layers, current accidentally starts flowing on the surface of the crack because the surface is fresh, and no native oxide layer prohibits the current flow. Once surface current flows, the PZT film starts melting locally because of the large current flow. The phenomenon can be seen as short circuit between the upper and lower electrodes, which becomes a trigger that gives rise to short circuit between the PZT film's melted point and the electrode of the device. That phenomenon completes within a very short period of time, so it is difficult to directly observe how the PZT film fractures in the experiment. In this study, although all were indirect evidence, with the experimental findings, the reasonable fracture mechanism of the PZT MEMS devices could be illustrated.

5. Conclusions

In this paper, we conducted two different types of cyclic loading test to experimentally understand the fracture mechanism of MEMS devices equipped with a PZT film actuator made by the sol-gel method. Two types of PZT MEMS device were prepared, namely, cantilever type

and clamped capacitor type, for cyclic mechanical and electrical loading tests, respectively. In the mechanical loading tests of the cantilever devices, it was found that the withstand voltage of the PZT MEMS devices decreased monotonically with increasing number of mechanical loading cycles. The cross-sectional observation result of the failed device showed that the PZT film cracked and melted. In the electrical loading tests of the clamped capacitor-type devices, the withstand voltage also decreased with increasing voltage amplitude during cyclic electrical loading. We found that the origin of the short circuit causing electrical failure was definitely different from that of cracking. Through the withstand voltage evaluation experiments of the clamped capacitor-type device with an FIB-processed artificial defect, it was clarified that cracking occurred first, followed by short circuit. This finding indicated that cracks generated in the PZT film became a trigger for introducing electrical short circuit. To extend the lifetime of PZT MEMS actuators, defects leading to cracking should be reduced or the PZT film should be toughened.

References

1 E. Hong, S. Trolier-McKinstry, R. L. Smith, S. V. Krishnaswamy, and C. B. Freidhoff: J. Microelectromech. Syst. **15** (2006) 4. https://doi.org/10.1109/JMEMS.2006.879122
2 M.F.M. Sabri, T. Ono, S. M. Said, Y. Kawai, and M. Esashi: J. Microelectromech. Syst. **24** (2015) 1. https://doi.org/10.1109/JMEMS.2014.2317495
3 A. Frangi, A. Opreni, N. Boni, P. Fedeli, R. Carminati, M. Merli, and G. Mendicino: J. Microelectromech. Syst. **29** (2020) 6. https://doi.org/10.1109/JMEMS.2020.3022557
4 A. Piot, J. Pribosek, J. Maufay, J. Schicker, A. Tortschanoff, R. Matloub, P. Muralt, and M. Moridi: J. Microelectromech. Syst. **30** (2021) 2. https://doi.org/10.1109/JMEMS.2021.3054357
5 H. Chen, S. Yu, H. Liu, J. Liu, Y. Xiao, D. Wu, X. Pan, C. Zhou, Y. Lei, and S. Liu: Microsyst. Nanoeng. **7** (2021) 55. https://doi.org/10.1038/s41378-021-00274-x
6 M. Jia, Q. Xu, D. Zhai, M. Yan, S. Jiang, M. Tang, D. Zhang, W. Zhu, and Y. Zhang: Crystals **1**3 (2023) 855. https://doi.org/10.3390/cryst13060855
7 J. C. Park, J. Y. Park, and Y-P. Lee: J. Microelectromech. Syst. **19** (2020) 5. https://doi.org/10.1109/JMEMS.2010.2067431
8 K. Wasa, T. Matsushima, H. Adachi, I. Kanno, and H. Kotera: J. Microelectromech. Syst. **21** (2012) 2. https://doi.org/10.1109/JMEMS.2011.2181156
9 L. Deng, Z. Wen, X. Zhao, C. Yuan, G. Luo, and J. Mo: J. Microelectromech. Syst. **23** (2014) 4. https://doi.org/10.1109/JMEMS.2013.2296034
10 A. Lei, R. Xu, L. M. Borregaard, M. Guizzetti, O. Hansen, and E. V. Thomsen: J. Microelectromech. Syst. **23** (2014) 4. https://doi.org/10.1109/JMEMS.2013.2295625
11 X. Dong, Z. Yi, L. Kong, Y. Tian, J. Liu, and B. Yang: J. Microelectromech. Syst. **28** (2019) 4. https://doi.org/10.1109/JMEMS.2019.2920213
12 C. Chen, S. B. Raghunathan,Z. Yu, M. Shabanimotlagh, Z. Chen, Z-Y. Chang, S. Blaak, C. Prins, J. Ponte, E. Noothout, H. J. Vos, J. G. Bosch, M. D. Verweij, N. de Jong, and M. A. Pertijs: IEEE Trans. Ultrason. Ferroelectr. Freq. Control **63** (2016) 1. https://doi.org/10.1109/TUFFC.2015.2496580
13 K. Zou, Q. Yue, J. Li, W. Zhang, R. Liang, and Z. Zhou: Ultrasonics **132** (2023) 107013. https://doi.org/10.1016/j.ultras.2023.107013
14 K. Kanda, I. Kanno, H. Kotera, and K. Wasa: J. Microelectromech. Syst. **18** (2009) 3. https://doi.org/10.1109/JMEMS.2009.2015478
15 V. Shih, S. Cheng, Y-R. Lin, A. Lin,Y-J. Liao,C-H. Lin,F-C. Huang, K. Tai, F. Hu,Y-H. Tsai, Y-W. Chen, K-F. Chang, C-H. Chiu, L. Tsai, V. Teng, C-M. Chen, T. Yu, Y-L. Tu, L-C. Tseng, J. Lee, B. Chen, S-F. Huang, and A. Kalnitsky: Proc. 20th Int. Conf. Solid-State Sensors, Actuators and Microsystems (Transducers 2019 - EUROSENSORS XXXIII, Berlin, 2019) 23–27. https://doi.org/10.1109/TRANSDUCERS.2019.8808685
16 R. M. Proie, R. G. Polcawich, J. S. Pulskamp, T. Ivanov, and M. E. Zaghloul: J. Microelectromech. Syst. **20** (2011) 4. https://doi.org/10.1109/JMEMS.2011.2148160

17 R. R. Benoit, R. Q. Rudy, J. S. Pulskamp, and R. G. Polcawich: J. Microelectromech. Syst. **29** (2020) 5. https://doi.org/10.1109/JMEMS.2020.3008201
18 T. Namazu, Y. Tashiro, and S. Inoue: J. Microelectromech. Syst. **17** (2007) 1. https://doi.org/10.1088/0960-1317/17/1/020
19 T. Namazu, A. Hashizume, and S. Inoue: Sens. Actuators, A **139** (2007) 1. https://doi.org/10.1016/j.sna.2006.10.047
20 T. Namazu, S. Ito, S, S. Kanetsuki, and S. Miyake: Jpn. J. Appl. Phys. **56** (2017) 6S1. https://doi.org/10.7567/JJAP.56.06GN11
21 S. Kanetsuki, S. Miyake, and T. Namazu: Sens. Mater. **31** (2019) 1. https://doi.org/10.18494/SAM.2019.2076
22 A. Mazzalai, D. Balma, N. Chidambaram, R. Matloub, and P. Muralt: J. Microelectromech. Syst. **24** (2015) 4. https://doi.org/10.1109/JMEMS.2014.2353855
23 D. M. Diniz Reis, S. Rzepka, and K. Hiller: Proc. 20th International Conference on Solid-State Sensors, Actuators and Microsystems (Transducers 2019 - EUROSENSORS XXXIII, Berlin, 2019) 1491–1494. https://doi.org/10.1109/TRANSDUCERS.2019.8808685
24 B. Akkopru-Akgun, W. Zhu, C. A. Randall, and M. T. Lanagan: APL Mater. **7** (2019) 12. https://doi.org/10.1063/1.5115391
25 R. P. Dahl-Hansen, J. M. Polfus, E. Vollestad,B. Akkopru-Akgun, L. Denis, K. Coleman, F. Tyholdt, S. Trolier-McKinstry, and T. Tybell: J. Appl. Phys. **127** (2020) 24. https://doi.org/10.1063/5.0003989
26 K. Coleman, J. Walker, W. Zhu, S. W. Ko, P. Mardilovich, and S. Trolier-McKinstry: Proc. 2020 Joint Conf. IEEE Int. Frequency Control Symp. and International Symposium on Applications of Ferroelectrics (IFCS-ISAF, Keystone, USA) 1–5. https://doi.org/10.1109/IFCS-ISAF41089.2020.9234833
27 R. P. Dahl-Hansen, F. Tyholdt,J. Gjessing, A. Vogl, P. Wittendorp, J. Vedum, and T. Tybell: J. Microelectromech. Syst. **30** (2021) 1. http://dx.doi.org/10.1109/JMEMS.2020.3031201
28 K. Coleman, R. Bermejo, D. Leguillon, and S. Trolier-McKinstry: Acta Mater. **191** (2020). https://doi.org/10.1016/j.actamat.2020.03.030
29 W. Zhu, B. Akkopru-Akgun, J. I. Yang, C. Fragkiadakis,K. Wang, S. W. Ko, and P. Mardilovich: Acta Mater. **219** (2021) 117251. https://doi.org/10.1016/j.actamat.2021.117251
30 N. Aruchamy, T. Schenk,V. Kovacova, S. Glinsek, E. Defay, and T. Granzow: J. Eur. Ceram. Soc. **41** (2021) 14. https://doi.org/10.1016/j.jeurceramsoc.2021.07.010
31 K. Coleman, M. Ritter. R. Bermejo, and S. Trolier-McKinstry: J. Eur. Ceram. Soc. **41** (2021) 4. https://doi.org/10.1016/j.jeurceramsoc.2020.11.002
32 B. Akkopru-Akgun,T. J. M. Bayer, K. Tsuji, C. A. Randall, M. T. Lanagan, and S. Trolier-McKinstry: Acta Mater. **208** (2021) 116680. https://doi.org/10.1016/j.actamat.2021.116680
33 B. Akkopru-Akgun, D. M. Marincel, K. Tsuji, T. J. M. Bayer, C. A. Randall, M. T. Lanagan, and S. J. Trolier-McKinstry: J. Am. Ceram. Soc. **104** (2021) 10. https://doi.org/10.1111/jace.17891
34 T. Namazu, Y. Isono, and T. Tanaka: J. Microelectromech. Syst. **9** (2000) 4. https://doi.org/10.1109/84.896765
35 T. Namazu, Y. Isono, and T. Tanaka: J. Microelectromech. Syst. **11** (2002) 2. https://doi.org/10.1109/84.993447
36 K. Wakamoto, K. Fuji, T. Otsuka, K. Nakahara, and T. Namazu: Exp. Tech. (2023). https://doi.org/10.1007/s40799-023-00664-y